Intelligent Positioning System for Magnetic Sensor Based Autonomous Vehicle

Young-Jae Ryoo
Dept. of Control System Eng.,
Mokpo National University,
Jeonnam 534-729, Korea
E-mail : yjryoo@mokpo.ac.kr

Eui-Sun Kim
Dept. of Electrical Eng.,
Seonam University,
Jeonbuk 590-711, Korea
E-mail : eskim@seonam.ac.kr

Young-Cheol Lim
Dept. of Electrical Eng.,
Chonnam National University,
Gwangju 500-757, Korea
E-mail : yclim@chonnam.ac.kr

Jai-Kyun Mok
New-energy Urban Train Team,
Korea Railroad Research Institute,
Kyounggi 437-050, Korea
E-mail : jkmok@krri.re.kr

Seky Chang
New-energy Urban Train Team,
Korea Railroad Research Institute,
Kyounggi 437-050, Korea
E-mail : seky@krri.re.kr

***Abstract*—In this paper, a position sensing system using magnet and magnetic sensor for autonomous vehicle is designed. Magnetic sensing is a reliable technology that has been developed for the purposed of position measurement and guidance, especially for applications in autonomous vehicle. The magnetic fields from a sample magnet are first measured to determine the characteristics of the field patterns as the basis for detection and position identification. A discussion of a position sensing system with a rejection algorithm of background field is presented. The position sensing technique was implemented in the guidance of autonomous vehicle. The results of lateral motion control show that position sensing system can be useful for an autonomous vehicle.**

Keywords- Position sensing system; Magnetic sensor; Autonomous vehicle

I. INTRODUCTION

In an autonomous vehicle, position sensing is an important task for the identification of vehicle's locations, such as the lateral position relative to a lane or a desired trajectory. Technologies developed for identifying the vehicle's location include electrically powered wire, computer vision, magnetic sensing, optical sensing, inertia navigation, and global positioning systems [1-3]. This paper focuses on magnetic sensing systems [4-7] that are used for ground vehicle control and guidance.

The magnetic marking scheme has several advantages compared with the electrified wiring scheme. Since it is a passive system, it is simple and does not use any energy. A vision sensing scheme is expensive to acquire and to process the optical images into credible data in real-time in any weather and road conditions. In the positioning reference system, magnets are embedded just under the surface of a road as Figure 1 shows. The magnetic fields generated by these magnets are detected by magnetic sensor mounted under the bumpers of the test vehicle.

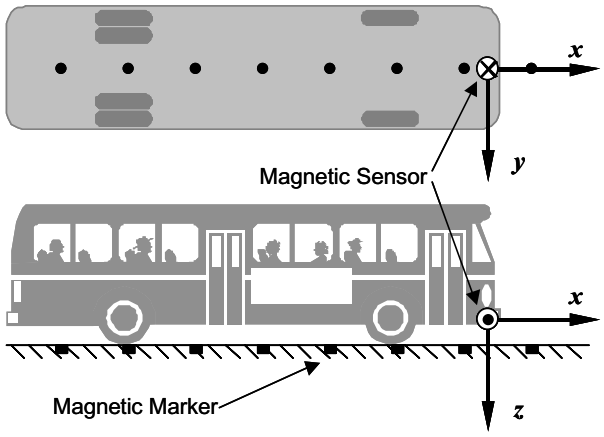

Figure 1. Position sensing system using magnetic sensor and magnets.

The major concern in implementing a magnetic sensing system on roads is the background magnetic field. For magnetic sensing, it is a problem that the magnitude of the background magnetic field is not small compared to that of the magnet's magnetic field. The background field may be stable or varying, depending on the specific location or the orientation.

This paper suggests a design of the position sensing system with a rejection algorithm of the background magnetic field, and discusses the related technical issues. In this paper, the position sensing technique is first illustrated in Section 2 by introducing the magnetic patterns produced by a sample magnet. An approach to reject the background magnetic field and algorithms are discussed in Section 3. The lateral motion control using a test vehicle is reported in Section 4. The paper concludes with a discussion of these concerns in Section 5.

II. POSITION SENSING SYSTEM

A. Analysis of Magnetic Fields of a Magnet

In this section, the comprehensive analysis of the magnetic field of a magnet used for position sensing is presented. Since a typical magnet has the shape of a cylindrical permanent magnet, assume that the magnet is a magnetic dipole. The magnetic field around a magnet can be described using rectangular coordinates as (see Figure 2) [8]:

$$B_x = \frac{3k_m zx}{(x^2 + y^2 + z^2)^{5/2}} \quad (1)$$

$$B_y = \frac{3k_m yz}{(x^2 + y^2 + z^2)^{5/2}} \quad (2)$$

$$B_z = \frac{k_m(2z^2 - x^2 - y^2)}{(x^2 + y^2 + z^2)^{5/2}}. \quad (3)$$

where

$$k_m = \frac{\mu_0 M_T}{4\pi}. \quad (4)$$

k_m is a constant proportional to the strength of the magnet.

$$M_T = \pi b^2 M_0 \quad (5)$$

where M_0 is the magnetization surface charge density, and b is the radius of the cylindrical permanent magnet.

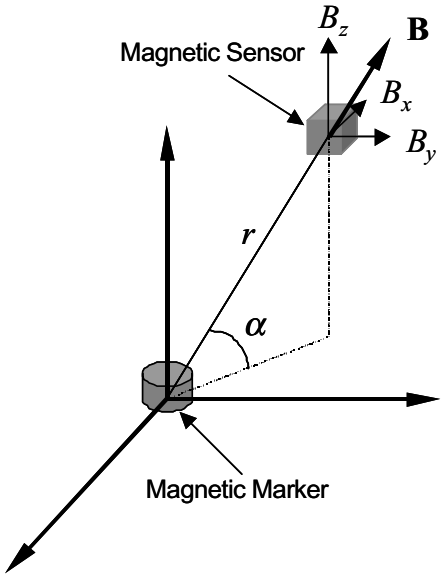

Figure 2. Magnetic field measured at a sensing position in rectangular coordinates.

Figure 2 depicts the three-axis components of the magnetic fields using rectangular coordinates. The longitudinal component (B_x) is parallel to the line of magnet installation on the road, the vertical component (B_z) perpendicular to the surface, and the lateral component (B_y) perpendicular to the other two axes. The longitudinal, the lateral, and the vertical component of the magnetic field can be transformed from the polar coordinate equations as:

As (1), (2) and (3) show, each component of the field is a function of the strength (k_m), the longitudinal (x), the lateral (y), and the vertical (z) distance to the sensor.

To verify that these model equations of (1), (2), and (3) represent the physical magnetic fields, the equations are compared with the direct experimental measurement using a ruler on the x-y test bench table. The magnetic sensor was mounted in a plane above 12.5 cm from the upper end of the magnet.

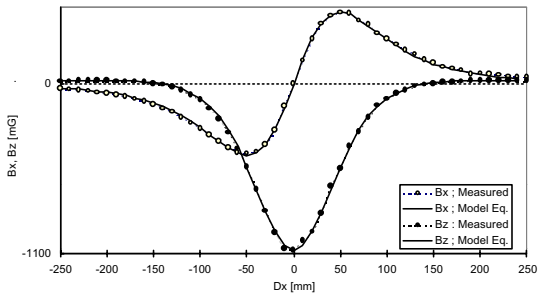

Figure 3. Comparison of the model equations with the direct measurement using a ruler.

Figure 3 shows the comparison of the magnetic field components calculated by the magnetic model equations with those measured by the experiment at various distances to the magnet. The data shows that these model equations are very accurate with the maximum error of only 13 mG along longitudinal (B_x), and 28 mG along vertical magnetic field (B_z). Thus, the assumption of a dipole magnet is reasonable, and the model equations are useful to represent the magnetic field.

The experimental data collected from magnet tests are presented for a comprehensive analysis of the magnetic fields. The first set of data was collected from a static test on a bench table. The sample magnet is made of ceramic material in a cylindrical shape with a diameter of 2.5 cm and a depth of 1 cm. The axis of the cylinder is placed perpendicular to the surface of the bench table. The measurements took place with a magnetic sensor at several different heights from the surface of the table to acquire a representative map of the magnetic field. For illustration, the data with the sensor at 7.5 cm height is shown in Figure4, 5, and 6.

These figures show composite curves with data from the three axes plotted along the distance from the magnet. The curves are generated with the origin at the location of the magnet. Notice how the three components change over space. Each curve represents the measurements at one cross

section along the longitudinal axis (x -axis), while multiple curves in each plot represent the measurement at various locations along the lateral axis (y -axis). The change of the magnetic fields along these three axes can be clearly identified.

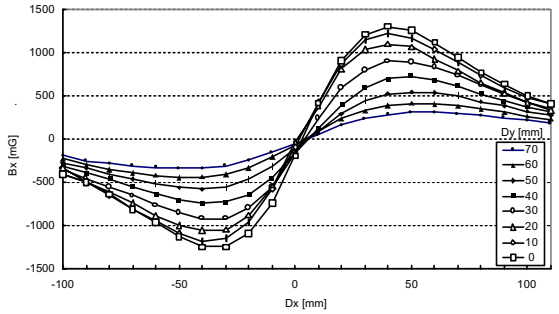

Figure 4. Longitudinal component of magnetic field of a magnet with sensor at 7.5 cm high.

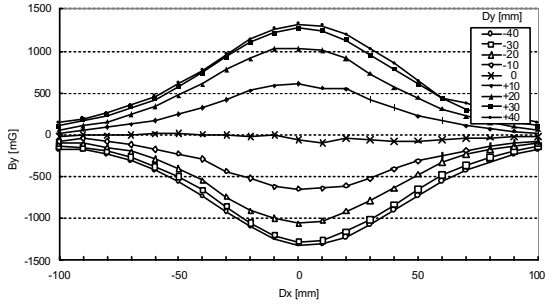

Figure 5. Lateral component of magnetic field of a magnet with sensor at 7.5 cm high.

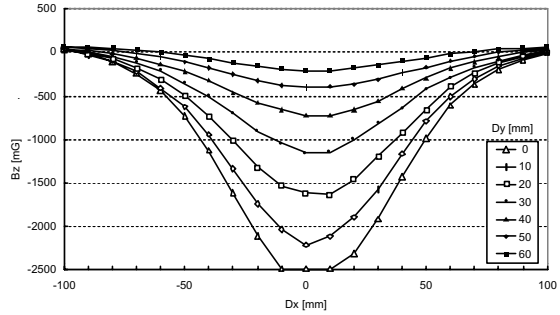

Figure 6. Vertical component of magnetic field of a magnet with sensor at 7.5 cm high.

In Figure 4, the longitudinal component (B_x) rises from zero at the center of the magnet and reaches its peak at a distance about 40 mm from the magnet, then gradually weakens farther away from the magnet. The peak value for this data set is about 1.2 G. The longitudinal field makes a steep transition near the magnet as it changes its sign. This steep transition becomes meaningful in interpreting the point at which a sensor passes over a magnet location.

As shown in Figure 5, the lateral component (B_y) reaches its peak at the top of the magnet, and drops down to zero at about 100 mm away from the magnet. The peak value for the data set of lateral component is about 1.2 G. In any horizontal plane parallel to that of the magnet, as a function of distance from the magnet, the patterns of B_x and B_y measurements are similar.

In Figure 6, the vertical field (B_z) is the strongest right at the top of the magnet, and diminishes to zero at about 100 mm away from the magnet. The peak value is above 2.5 G for the data set in Figure 6, but cannot be measured due to the magnetic sensor limitations. The vertical field quickly drops as it moves away from the magnet. Since the vertical field is the strongest component among the measurements near the magnet, its use will be significant in identifying the closeness of a magnet.

B. Position Sensing from Magnetic Fields

Once the magnetic fields are measured, the measured fields at that location will be used to identify the distance to the magnet.

From (5), (6) and (7), the sensor position (x , y) can be derived as:

$$x = \left\{ \frac{3k_m(3B_z + C)256{B_x}^3}{(24{B_x}^2 + 24{B_y}^2 + 18{B_z}^2 + 6B_zC)^{5/2}} \right\}^{1/3} \quad (6)$$

$$y = \frac{B_y}{B_x} x \quad (7)$$

where

$$C = \pm\sqrt{8{B_x}^2 + 8{B_y}^2 + 9{B_z}^2} \,. \quad (8)$$

According to equations (6), (7), and (8), the position of the sensor with respect to the magnets can be calculated. The inverse mapping equations are useful to estimate the position continuously as long as the magnetic field is strong enough to be sensed. In the implemented system, the transformation of the measured signals to the distance to the magnet is based on the inverse mapping relationship.

Figure 7 shows a sample of inverse mapping of the measured field strengths at a longitudinal field of 0 mG. The data points are produced with the data from equations (6), (7), and (8). Measurements from the magnetic field components produce a distance simply. These curves in Figure 7 constitute a basis for position identification. In the implementation, the curves as seen in Figure 7 are calculated in the signal-processing program. However, in a practical system, it should be noted that the magnitude of the background magnetic field is not small compared to that of the magnet magnetic field.

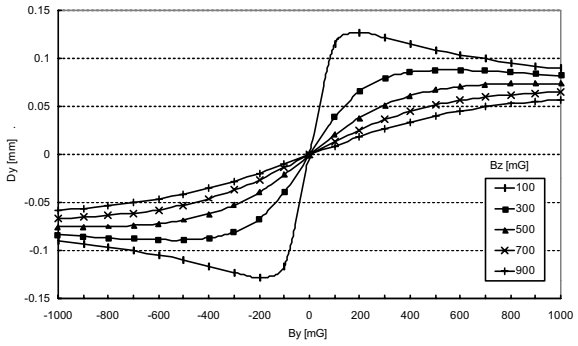

Figure 7. Vertical component of magnetic field of a magnet with sensor at 7.5 cm high.

III. REJECTION OF BACKGROUND MAGNETIC FIELD

A. Properties of Background Magnetic Fields

The major concern in implementing a magnetic sensing system on roads is the background field. The background field may be stable or varying, depending on the specific vehicle's location or the orientation. In this section, we examine the properties of the background magnetic field on the field patterns generated by the magnets.

The data were taken from a static test similar to that mentioned in the previous section, but without the magnet. A robot arm with an attached magnetic sensor and data acquisition system was used to acquire the background field at a variety of orientations. The sensor was mounted in the gripper of the robot arm. The orientation of the sensor could be changed continuously by the operation of the robot. The sensor was approximately 7.5 cm above the ground.

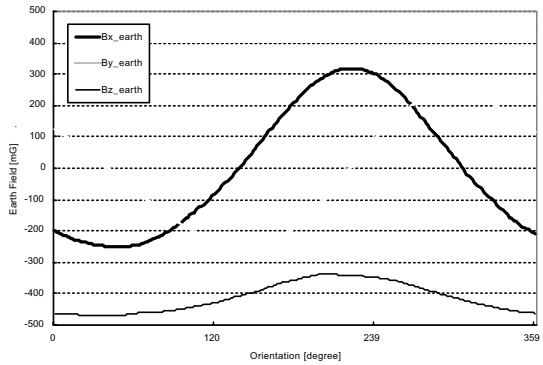

Figure 8. Patterns of the background magnetic field along the variation of the orientation of the sensor.

Figure 8 shows the longitudinal, lateral and vertical fields generated by the background magnetic field as a function of the orientation of the sensor. The curves are generated with the origin at an initial orientation of the sensor. Notice that the phase of the longitudinal component (B_{x_earth}) leads by 90 degrees compared to that of the lateral component (B_{y_earth}). The vertical component (B_{z_earth}) is almost constant. The longitudinal and lateral components are changing depending upon the direction in which the vehicle is heading.

In Figure 8, it was demonstrated by the sampled data sets that the ground field show significant variations of magnitude and phase. As a result, the calculation of the background field is by no means trivial. Since the background magnetic field changes with the vehicle's orientation, it does require a rejection algorithm for the background field. An error in the value of the background field can result in totally incorrect interpretation of the measured fields. Since sensing algorithms are based on the pattern of magnetic fields near the magnet, it is essential to take great care taking into account the background magnetic field.

B. Rejection Techneque of Background Field

In magnetic sensing, it is a problem that the magnitude of the background magnetic field is not small compared to that of the magnet magnetic field. Thus, the signal processing for the described position measurement application involves two tasks: 1) the rejection of the background field, and 2) the inverse mapping of processed signals to a position relative to the magnet. In this section, several rejection algorithms of the background magnetic field for position identification are presented with a discussion of related technical issues.

Once the background fields are removed, the remaining portions of the signals represent the fields generated from the expected magnet. From the remaining signal, the position of the magnet could be determined by the inverse mapping equation.

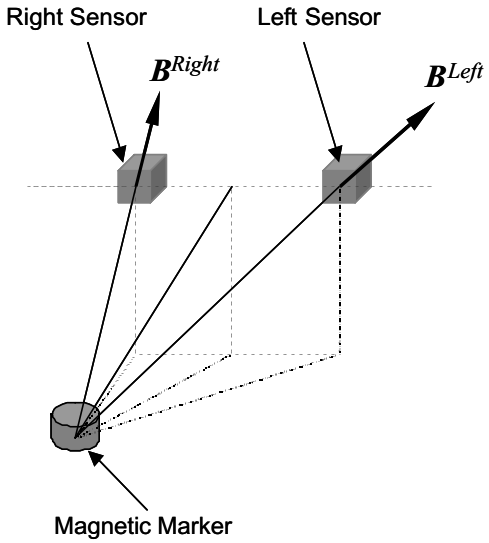

Figure 9. The earth's field rejection using dual sensors.

A new approach was suggested to reject the earth's fields by assuming that the earth's field is approximately uniform in a small region. This method uses two nearby sensors to eliminate the common background components by taking the difference between the dual sensors. It is based on the assumption that the background fields are

approximately the same at the two sensor locations. The two sensors line up horizontally on the bumper of the vehicle and are located at the same height as shown in Fig. 11. Thus, the measured fields at two close points can be expressed as

$$B^{Left}(t) = B^{Left}_{magnet} + B^{Left}_{earth} + B^{Left}_{local} \qquad (9)$$

$$B^{Right}(t) = B^{Right}_{magnet} + B^{Right}_{earth} + B^{Right}_{local} \; . \qquad (10)$$

The earth's field is typically much greater than the local disturbances caused by the two sensors being positioned slightly apart. Therefore, a difference is taken from the two observation points

$$\begin{aligned} \Delta B(t) &= B^{Left}(t) - B^{Right}(t) \\ &\approx B^{Left}_{magnet} - B^{Right}_{magnet} \end{aligned} \qquad (11)$$

The earth's field is directly removed. A process of correlating the calculated difference (ΔB) of the measurement location is similar to the exercise that was described in the inverse mapping.

IV. Experiment of Positioning System

A. Test Setup

The tests of the proposed method using the compass sensor, and the lateral control tests were conducted using a test vehicle. The test vehicle is a typical rear-wheel-driven half-size passenger car. The vehicle was equipped with two magnetic sensors. The two sensors are aligned vertically, 30 cm apart, and located on the front bumper as shown in Figure 10. The vehicle velocity was measured by a wheel encoder signal.

The developed system was implemented on an IBM-PC (2GHz Pentium4 processor) with Windows XP. The interface to the sensors and the actuator was through a National Instruments data acquisition board. The data sampling and the control were running with a 14 msec loop time. The control itself does not need 14 msec loop time. However, 14 msec loop time was chosen to pick up as much data as possible from each magnet since the measurement range from the magnetic field is only ± 30 cm in this case.

Figure 10. Photograph of the vehicle on the test track.

B. Position Sensing

The position sensing tests were performed on a test track. The shape of the test track is as shown in Figure 11. Much of the test track was based upon a previously existing dirt road at the site. The track is approximately 38 meter long. The permanent magnets, with 2.2 cm diameter and 1 cm depth, were installed along the center of the track at 30 cm spacing.

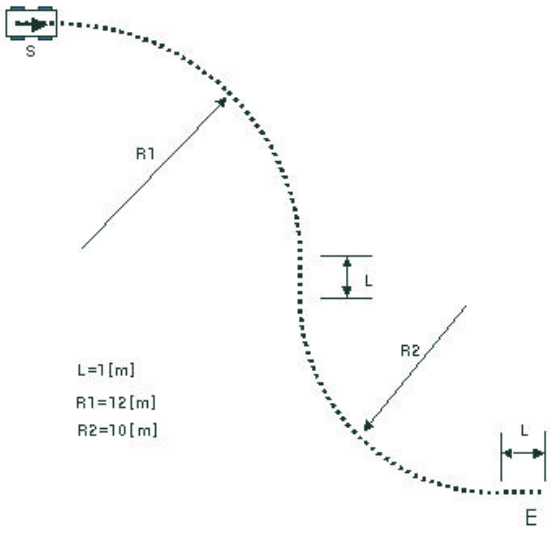

Figure 11. The layout of the test track.

Figure 12 shows the result of the test on the test track using the rejection algorithm of dual sensor and the position sensing system developed in this study. Although the road is smooth, the road curvature changes stepwise sharply from one direction to the opposite, and the measured magnetic field is changed at 12 second as shown in Figure 12 (a), (b), and (c).

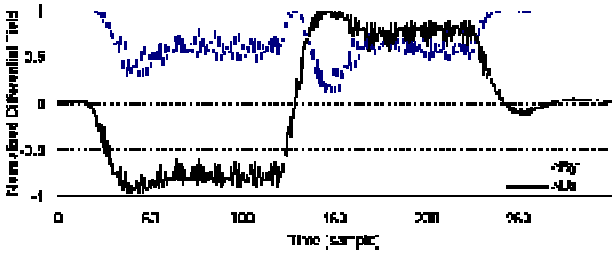

(a)

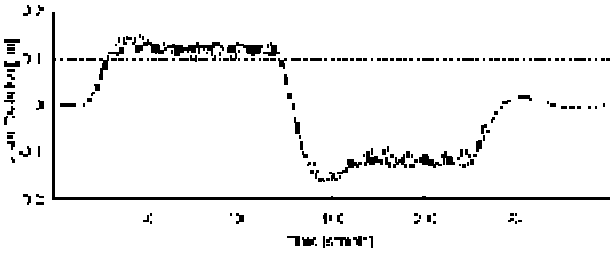

(b)

Figure 12. The test result of positioning. (a) the differences of magnetic field, (b) the estimated lateral position.

The positioning algorithm, proposed in this paper, was adapted for the control system. After the rejection of the background field using the dual sensor, only the field from the magnets remains. According to the inverse mapping, the position of the sensor installed in the vehicle relative to the magnet was calculated. The lateral error of the vehicle from the center of the road is produced. A simple and fast PD based control is used to demonstrate the practical steering of the vehicle. The input of the controller is the lateral error, and the output of the controller is the steering angle.

V. CONCLUSION

In this paper, a position reference system using a magnetic sensor and magnet was discussed. The field patterns of a sample magnet were first measured to illustrate the basic characteristics of such systems. The properties of the background field were then examined by conducting experiments at different geometric orientations. The observations from these experiments revealed that indeed there were potential complications that might be caused by the vehicle's position and orientation. These effects must be handled carefully to ensure a robust sensing approach for correct identification of the vehicle's position.

The lateral motion control of the test vehicle shows that it is reliable to sense the vehicle's position from the magnetic field on the real track. The suggested design of position sensing system was working well on a road with high curvature. When the deployment of magnetic sensing systems for position reference increases, these subjects deserve elaborated studies and thorough analysis.

ACKNOWLEDGEMENT

This paper was supported by "National Transportation Key Technology R&D Project".

REFERENCES

[1] Shumeet Baluja, Evolution of an artificial neural network based autonomous land vehicle controller, IEEE Transactions on Systems, Man, and Cybernetics - Part B: Cybernetics, vol. 26, no. 3, pp. 450-463, June 1996.

[2] Kevin M. Passio, Intelligent control for autonomous vehicle, IEEE Spectrum, pp. 55-62, June 1995.

[3] Ronald K. Jurgen, Smart cars and highways go global, IEEE Spectrum, pp. 26-36, May 1991.

[4] James G. Bender, An overview of system studies of automated highway systems, IEEE Transactions on vehicular technology, vol. 40, no. 1, Feb. 1991.

[5] Seibum B. Choi, The design of a look-down feedback adaptive controller for the lateral control of the front-wheel-steering autonomous vehicles, IEEE Trans. Veh. Technol., vol. 49, no. 6, pp.2257-2269, Nov. 2000.

[6] Ching-Yao Chan, Magnetic sensing as a position reference system for ground vehicle control, IEEE Trans. Inst. and Meas., vol. 51, no. 1, pp.43-52, Dec. 2002.

[7] Han-Shue Tan, J. Guldner, S. Patwardhan, Chieh Chen, and B. Bougler, Development of an automated steering vehicle based on road magnets - a case study of mechatronic system design, IEEE/ASME Transactions on Mechatronics, vol. 4, no. 3, pp.258-272, Sept. 1999.

[8] E. S. Shire, Classical electricity and magnetism, Cambridge, U.K.: Cambridge University Press, 1960.